SAND2000-0985J

Effective index model predicts modal frequencies of vertical-cavity lasers

Darwin K. Serkland, G. R. Hadley, K. D. Choquette, K. M. Geib, and A. A. Allerman

Sandia National Laboratories, P.O. Box 5800, MS 0603, Albuquerque, NM 87185

Phone: (505) 844-5355; Fax: (505) 844-8985; E-mail: dkserkl@sandia.gov

Abstract

Previously, an effective index optical model was introduced for the analysis of lateral waveguiding effects in vertical-cavity surface-emitting lasers. We show that the resultant transverse equation is almost identical to the one typically obtained in the analysis of dielectric waveguide problems, such as a step-index optical fiber. The solution to the transverse equation yields the lateral dependence of the optical field and, as we recognize in this paper, the discrete frequencies of the microcavity modes. As an example, we apply this technique to the analysis of vertical-cavity lasers that contain thin-oxide apertures. The model intuitively explains our experimental data and makes quantitative predictions in good agreement with a highly accurate numerical model.

(Draft 3/3/00. For submission to APL.)

As vertical-cavity surface-emitting laser (VCSEL) technology matures, more complicated optical microcavity structures are being designed. In order to aid the design process, various predictive numerical models have been developed, ranging from beam propagation methods to sophisticated finite difference models.[1-7] The recently introduced effective index model[4] is especially intuitive, because of its similarity to well-known dielectric waveguide problems, and is computationally efficient, since it condenses the complicated vertical structure and leaves only a transverse equation to be solved. Previously the effective index model was shown to determine the electric field profile in a microcavity.[4]

In this paper, we demonstrate that the effective index model also predicts the allowed modal frequencies of a microcavity. As an example, we analyze the case of VCSELs that employ thin-oxide apertures.[8,9] We find good agreement with the experimental data and with the predictions of a more sophisticated finite-difference model.[7] Exploiting the close analogy between oxide-aperture VCSELs and step-index optical fibers, we determine the maximum aperture size for which the VCSEL will support only a single transverse mode.

We start by comparing the effective index model of Ref. 4 with the conventional solution technique for optical waveguide problems. In both cases, we seek solutions of the scalar wave equation which have the separable form

$$E(\mathbf{x}, z, t) \approx E_i(\mathbf{x})\phi_i(z)\exp(-i\omega t)\,, \tag{1}$$

where $\mathbf{x} = (x, y)$ denotes the transverse coordinates, and the subscripts i denote different lateral regions, such as the core and cladding, within which the permittivity $\epsilon_i(z)$ is laterally invariant.

For waveguides that are uniform in z, it is conventional to take $\phi_i(z) = \exp(+i\beta z)$, which leads to the waveguide equation

$$\nabla_t^2 E_i(\mathbf{x}) + (\epsilon_i k_0^2 - \beta^2)E_i(\mathbf{x}) = 0\,, \tag{2}$$

where we introduced the transverse Laplacian $\nabla_t^2 = \partial^2/\partial x^2 + \partial^2/\partial y^2$ and the vacuum wavevector $k_0 \equiv \omega/c$. This is equivalent to the Schrödinger equation, and has been solved, with relevant continuity conditions on $E_i(\mathbf{x})$, for many waveguides of interest.[10]

DISCLAIMER

We now turn to the effective index model of a microcavity. A key assumption is that, within each region, $\phi_i(z)$ is the solution to the 1-dimensional wave equation

$$\frac{d^2}{dz^2}\phi_i(z) + \epsilon_i(z)k_{iz}^2\phi_i(z) = 0\,, \tag{3}$$

that describes an infinitely wide Fabry-Perot cavity with vertical structure determined by $\epsilon_i(z)$. Ignoring the imaginary part of k_{iz} that accounts for loss, we recognize that $k_{iz} = \omega_i/c$ is the vacuum wavevector corresponding to the Fabry-Perot resonance frequency ω_i. We note that the 1-dimensional wave equation (3) is routinely solved in the VCSEL community (often by means of a transmission matrix approach)[11], so we regard k_{iz} and $\phi_i(z)$ as known properties of each region i.

The effective index derivation follows Ref. 4 and the details will be discussed elsewhere. In short, we insert the solution (1) into the scalar wave equation and use the constraint (3) to obtain the effective index equation

$$\nabla_t^2 E_i(\mathbf{x}) + \langle\epsilon_i\rangle(k_0^2 - k_{iz}^2)E_i(\mathbf{x}) = 0\,, \tag{4}$$

where we assume the normalization $\int |\phi_i(z)|^2 dz = 1$ and define $\langle\epsilon_i\rangle \equiv \int \epsilon_i(z)|\phi_i(z)|^2 dz$, which represents the dielectric constant weighted by the longitudinal standing wave in each region i.

The effective index equation (4) is nearly identical to the waveguide equation (2). Both have the form

$$\nabla_t^2 E_i(\mathbf{x}) + h_i^2 E_i(\mathbf{x}) = 0\,, \tag{5}$$

where h_i is regarded as a transverse wavevector (in the medium) in region i, and the fields are oscillatory or decaying according to whether h_i^2 is positive or negative, respectively. The boundary conditions for the various regions constrain h_i^2 to assume only discrete values. For waveguides, any frequency ω may be chosen and the corresponding discrete values of the propagation constant β are determined by $\beta^2 = \epsilon_i k_0^2 - h_i^2$. In the case of the effective index model of a microcavity, the longitudinal component of the free-space wavevector is

prescribed in each region i by the local Fabry-Perot resonance wavevector $k_{iz} = \omega_i/c$. Hence, for each discrete value of h_i^2, the corresponding modal frequency ω is determined by

$$\frac{\omega^2}{c^2} = k_0^2 = \frac{h_i^2}{\langle \epsilon_i \rangle} + k_{iz}^2 , \tag{6}$$

and is independent of the particular region i considered in evaluating Eq. (6). The recognition that the effective index model precisely determines the allowed modal frequencies according to Eq. (6) is a key result of this paper.

Equation (6) motivates us to define for each region a vector $\mathbf{k_i}$, whose longitudinal component is $k_{iz} = \omega_i/c$ and whose transverse component k_{it} is given by $k_{it}^2 = h_i^2/\langle \epsilon_i \rangle = k_0^2 - k_{iz}^2$. The vector $\mathbf{k_i}$ has the virtue that its magnitude is fixed at k_0 in all regions; only its angle changes from one region to another. If we define the angle θ_i as the angle between the z axis and the vector $\mathbf{k_i}$, then $\cos(\theta_i) = k_{iz}/k_0$. Moreover, the invariance of k_0 leads to

$$2\pi/k_0 = \lambda_1 \cos(\theta_1) = \lambda_2 \cos(\theta_2) , \tag{7}$$

where we have introduced the Fabry-Perot resonance wavelengths $\lambda_i = 2\pi/k_{iz}$. Equation (7) is analogous to Snell's law, and hence we interpret the effective index in each region as being proportional to the resonance wavelength λ_i. Thus, modifications of a layer thickness that shift the Fabry-Perot resonance will effectively change the lateral index profile.

As a quantitative test of the effective index model, we consider a VCSEL microcavity that contains thin-oxide apertures for optical and current confinement.[9] Although the apertures in our VCSELs are square, we will approximate them as being circular of diameter $2a$ equal to the width of the square aperture. The VCSEL cross section is schematically depicted on the right side of Fig. 1(a). In the core region 1 ($r < a$), the vertical layer structure is that of a standard VCSEL at 850 nm. The λ cavity is bounded by many DBR periods (36 below and 21 above), each composed of two $\lambda/4$ AlGaAs layers containing 16% and 92% Al:As ratios, respectively. The only exceptions are the DBR periods immediately above and below the cavity, where the thickness of the high-index 16% layer is made $3\lambda/4$ so that a thin 98% layer can be inserted in it at a null in the vertical standing wave (see the

left side of Fig. 1(a)). The thin 98% layers are roughly $\lambda/8$ thick. After etching mesas to expose the edges of the layers, water vapor is used to laterally oxidize the thin 98% layers inward from the edge of the mesa to the radial position $r = a$. Oxidation reduces the index of the 98% layers from 3.0 to roughly 1.6. In addition to the core radius a, the only other quantities required to fully specify the effective index problem are the Fabry-Perot resonance wavelengths λ_i and the field-weighted permittivities $\langle\epsilon_i\rangle$, which are readily obtained from 1-dimensional simulations. The resonance wavelengths are found to be λ_1 =855.81 nm and $\lambda_2 = \lambda_1 - 1.54$ nm, and the corresponding permittivities are $\langle\epsilon_1\rangle$=10.98 and $\langle\epsilon_2\rangle = \langle\epsilon_1\rangle - 0.06$. The longitudinal wavevector components $k_{iz} = 2\pi/\lambda_i$ that satisfy the local Fabry-Perot resonance are plotted on the right side of Fig. 1(b).

The allowed frequencies $\omega = ck_0$ of guided modes are constrained by $k_{1z} < k_0 < k_{2z}$ ($\omega_1 < \omega < \omega_2$) so that the field is oscillatory in the core region 1 and decays toward infinity in the cladding region 2. At the interface between the two regions, continuity of the tangential components of the electric and magnetic fields yields two equations that determine two unknowns: (a) the ratio of the amplitude coefficients in the two regions and (b) the mode frequency $\omega = ck_0$. Although in general this procedure could be followed exactly, we will make another slight approximation. We note that the dominant behavior predicted by the effective index equation (4) is due to the difference $(k_0^2 - k_{iz}^2)$, and hence we assume that $\langle\epsilon_1\rangle \approx \langle\epsilon_2\rangle$.

The approximation that $\langle\epsilon_i\rangle = \langle\epsilon\rangle$ is independent of the region i allows us to make an exact correspondence with conventional step-index-fiber solutions, by assuring that

$$V^2 \equiv (h_1^2 - h_2^2)a^2 = \langle\epsilon\rangle(k_{2z}^2 - k_{1z}^2)a^2 \tag{8}$$

is a constant. Having identified the appropriate normalized frequency parameter V, we may directly use the known solutions for step-index optical fibers which are commonly presented as a function of V.[10,12]

Figure 2(a) shows the wavelength of the fundamental transverse mode versus aperture width for our thin-oxide VCSELs. The solid line corresponds to the effective index predic-

tions, which are determined by Eq. (6) in conjunction with the known solutions[12] for the normalized propagation constant $b \equiv 1-(h_1 a/V)^2$ versus V, and the relation $V = a\,1.46/\mu\text{m}$ for our thin-oxide VCSELs. As expected, the mode frequency approaches the cladding resonance as the aperture width shrinks to zero and the core resonance as the aperture increases to infinity. Uniform vertical expansion of the structure, obtained by increasing the epitaxial growth rate or heating the device, would yield a uniform offset of the wavelengths but leave the variation versus aperture width virtually unchanged. The effective index predictions agree almost exactly with those of an accurate 2-dimensional finite difference model,[7] shown by the circles in Fig. 2(a). The solid triangles in Fig. 2(a) indicate the actual VCSEL wavelengths, measured by driving the lasers 10% above threshold with 100-ns current pulses. The small discrepancy between the shape of the experimental and theoretical plots in Fig. 2(a) is most likely due to modeling the square apertures as circular and slightly underestimating the actual thickness of the oxide layers. Finally, we note that step-index optical fibers are known to support only a single mode when the normalized frequency satisfies $V < 2.405$, which is equivalent to $2a < 3.3\mu$m for our thin-oxide VCSELs. Experimentally, we find that the thin-oxide VCSELs operate in a single mode for square-aperture widths less than 2.5μm.

Figure 2(b) shows the fundamental-mode full width at half-maximum (FWHM) intensity as a function of aperture size. Again, the effective index prediction (solid line) closely tracks the finite-difference calculations (circles). Moreover, the experimental measurements (solid triangles) validate the numerical predictions. In contrast with thick oxide VCSELs, we see that the mode is not always confined within the aperture. In particular, as the core diameter is reduced below $1.5\,\mu$m we observe that the mode size actually increases and the mode spreads significantly into the cladding region.

A surprising feature of Fig. 2 is the continuous blue-shift of the mode wavelength as the aperture width decreases below $1.5\,\mu$m, in spite of the fact that the mode width increases. Conventional wisdom says that the transverse wavevector varies inversely with the mode width. Therefore, assuming a fixed longitudinal wavevector, it could be expected that the mode wavelength will vary monotonically with the mode width. Indeed, in the case of

thick-oxide VCSELs, where the mode remains almost entirely within the aperture, these expectations are confirmed by experiments.[13] In the case of small-aperture thin-oxide VCSELs, the paradox is resolved by noting that as the mode spreads into the oxidized region, the mode frequency must approach the resonance in the oxidized region. In fact, the effective index model predicts that as the aperture size is reduced, the transverse wavevector in the core region continues to increase, even as the mode width increases.

In summary, we have used the effective index model to obtain a simplified wave equation, whose solutions determine both the discrete modal frequencies and the transverse dependence of the optical field. Because the simplified wave equation is almost identical to the one obtained with the conventional approach to solving dielectric waveguide problems, known techniques and solutions can be applied directly to vertical-cavity lasers. As an example, we have analyzed the case of VCSELs incorporating thin-oxide apertures and we demonstrated close agreement with experimental data and with the predictions of a more sophisticated numerical model. The simplicity and intuitive aspects of the effective index model make it appropriate for the analysis of vertical-cavities with complicated lateral modulation of the layer thicknesses and/or indices.

Sandia is a multiprogram laboratory operated by Sandia Corporation for the U.S. Department of Energy under Contract No. DE-AC04-94AL85000.

REFERENCES

1. M. Shimizu, F. Koyama, K. Iga, IEICE Trans. **E74**, 3334 (1991).

2. J.-P. Zhang, K. Petermann, IEEE J. Quantum Electron. **30**, 1529 (1994).

3. C. Lin, D. Deppe, IEEE J. Lightwave Technol. **13**, 575 (1995).

4. G. R. Hadley, Opt. Lett. **20**, 1483 (1995).

5. L. Coldren, B. Thibeault, E. Hegblom, G. Thompson, J. Scott, Appl. Phys. Lett. **68**, 313 (1996).

6. H. Wenzel, H.-J. Wunsche, IEEE J. Quantum Electron. **33**, 1156 (1997).

7. G. R. Hadley, IEEE J. Lightwave Technol. **16**, 142 (1998).

8. A. E. Bond, P. D. Dapkus, and J. D. O'Brien, IEEE Photon. Technol. Lett. **10**, 1362 (1998).

9. K. D. Choquette, A. A. Allerman, H. Q. Hou, G. R. Hadley, K. M. Geib, and B. E. Hammons, Digest 16th International Semiconductor Laser Conference, p. 237 (1998).

10. D. Marcuse, Theory of Dielectric Optical Waveguides, 2nd edition (Academic Press, 1991).

11. L. A. Coldren, S. W. Corzine, Diode Lasers and Photonic Integrated Circuits (Wiley, 1995), appendix 7.

12. D. Gloge, Appl. Opt. **10**, 2252 (1971).

13. D. L. Huffaker and D. G. Deppe, IEEE Photon. Technol. Lett. **8**, 858 (1996).

FIGURES

Fig. 1. The right side of part (a) shows a schematic cross section of the thin-oxide VCSEL layers, starting at the center of the λ cavity and continuing upward through the first (P1) and second (P2) mirror periods. The hatched region indicates where the 98% layer has been oxidized. The left side of part (a) shows the vertical standing wave $|\phi_1(z)|^2$ in region 1. In part (b), the fundamental transverse mode frequency $\omega = ck_0$ is indicated on the right, and the corresponding electric field profile is shown on the left. On the right, we indicate how to graphically determine the transverse wavevector in region 1. For clarity, the separation between the Fabry-Perot resonance wavevectors k_{1z} and k_{2z} is exaggerated.

Fig. 2. The wavelength (a) and full width at half maximum (b) of the fundamental mode as a function of the oxide-aperture width. The solid triangles are the experimental data points and the solid line shows the predictions of the effective index model. For comparison, the circles show the predictions of accurate 2-dimensional finite-difference calculations.[7] The lower solid line in part (a) shows the wavelength prediction for the first higher-order transverse mode.

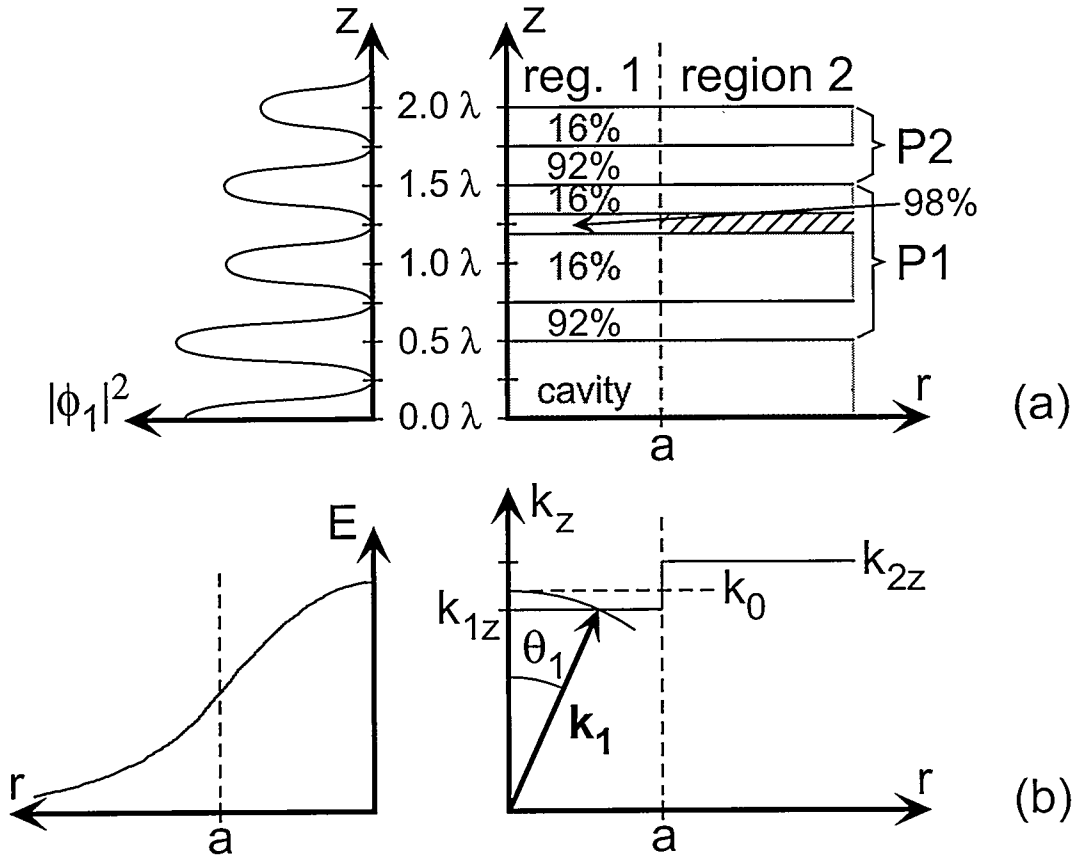

Fig. 1 D.K. Serkland et al.

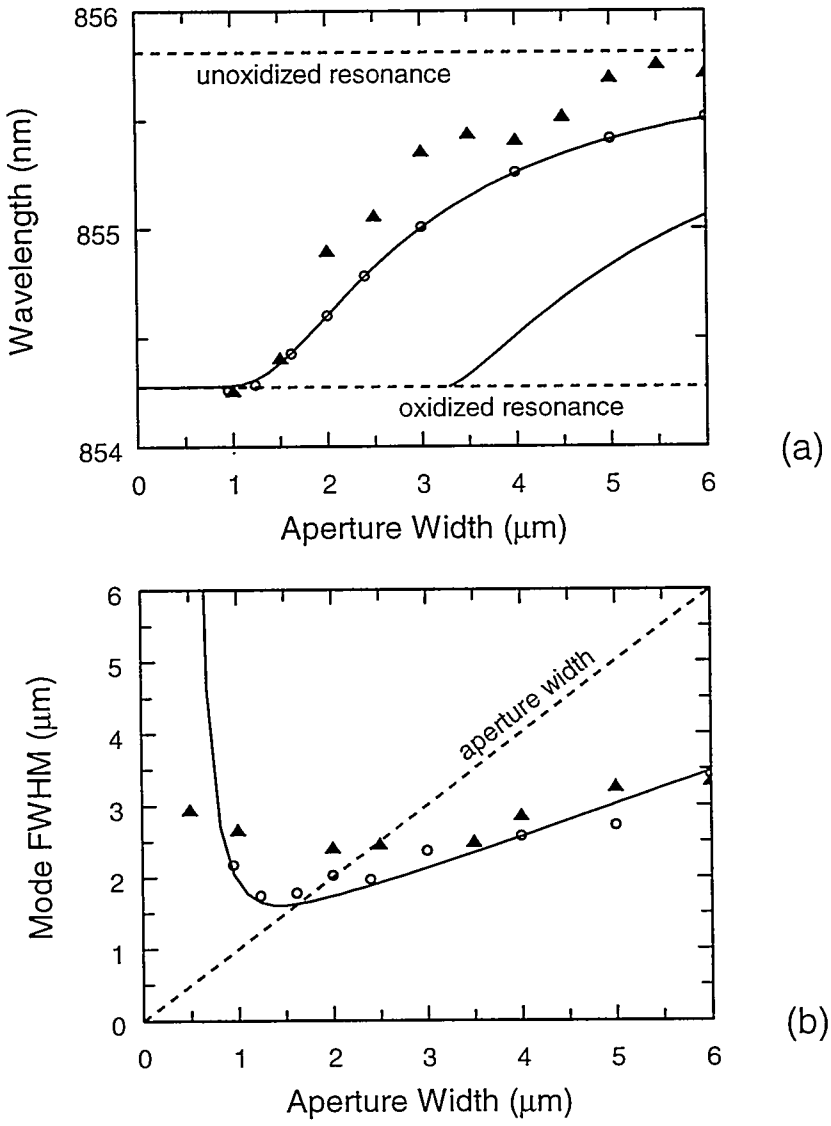

Fig. 2 D.K. Serkland et al.